Journal of Sound and Vibration 332 (2013) 608–621

Contents lists available at SciVerse ScienceDirect

Journal of Sound and Vibration

journal homepage: www.elsevier.com/locate/jsvi

Nonlinear dynamics of a rotordynamic nonsmooth shape memory alloy system

Leandro C. Silva [a], Marcelo A. Savi [a,*], Alberto Paiva [b]

[a] Universidade Federal do Rio de Janeiro, COPPE, Department of Mechanical Engineering, 21.945.970, Rio de Janeiro, RJ, Brazil
[b] Universidade Federal Fluminense, Escola de Engenharia Industrial e Metalúrgica de Volta Redonda, 27.255.250, Volta Redonda, RJ, Brazil

ARTICLE INFO

Article history:
Received 11 February 2012
Received in revised form
22 August 2012
Accepted 13 September 2012
Handling Editor: L.N. Virgin

ABSTRACT

This contribution deals with the analysis of a rotordynamic nonsmooth shape memory alloy (SMA) system. The rotor–bearing system is modeled as a Jeffcott rotor with two-degrees of freedom and discontinuous supports. Two different situations are investigated: linear elastic support and shape memory alloy support. Numerical simulations are carried out establishing a comparison between elastic and SMA systems, showing situations where nonlinear effects of SMAs are interesting in dynamical responses avoiding undesirable behaviors. Temperature dependence of SMA response is investigated showing adaptive aspects of this kind of system.

1. Introduction

Rotordynamical systems are employed in several devices as engines and turbines. Rotor–bearing interactions have attracted much attention from researchers not only due to their wide applicability in several fields, but also for their dynamical response richness. The modeling of rotor dynamical systems is related to different research efforts, being associated with signal analysis, finite element method, among other approaches [1–5].

Despite of recent sophisticated models, the simple sketch proposed by Jeffcott [6] is useful for nonlinear dynamical analyses. Karpenko et al. [7] studied the nonlinear dynamics of a rotor–bearing system modeled by an oscillator with two-degrees of freedom and discontinuous elastic supports. The physical system was based on a Jeffcott rotor and the work revealed a rich dynamic behavior of the system, including chaos. Pavlovskaia et al. [8] analyzed preloaded snubber ring subjected to out-of-balance excitation. Karpenko et al. [9] showed the correlation between numerical and experimental results promoting an understanding of this kind of system and its applicability. Shang et al. [10] investigated the global response of rotor–bearing system considering the effects of dry friction.

The Jeffcott rotor may be understood as a two-degree of freedom system with intermittent contacts that provides nonsmooth nonlinearities. Usually, this kind of nonlinearity appears in several engineering systems with discontinuous characteristics as contact or dry friction, being the objective of distinct researches that investigate the nonlinear dynamics of these systems [11–13].

Since nonsmooth systems present an unusual complex behavior, their description involves many mathematical and numerical difficulties. Therefore, proper mathematical approaches need to be developed, such as in Refs. [14–20]. Besides, experimental studies are of great importance for a better comprehension of nonsmooth systems and several researches were dedicated to this objective [20–28].

* Corresponding author.
E-mail addresses: savi@mecanica.ufrj.br (M.A. Savi), paiva@puvr.uff.br (A. Paiva).

0022-460X/$ - see front matter © 2012 Elsevier Ltd. All rights reserved.
http://dx.doi.org/10.1016/j.jsv.2012.09.018

The use of smart materials in rotordynamic systems is of special interest since they can provide better performance, avoiding several undesirable behaviors. Shape memory alloys (SMAs) represent an interesting alternative where adaptive characteristics and high dissipation capacity are required. Santos and Savi [29] and Sitnikova et al. [30] explored a one-degree of freedom version of the rotordynamical system represented by a primary oscillator with a secondary system (support) with an SMA element. These articles compared the elastic support responses with those obtained from an SMA support. In general, both articles showed several complex behaviors of this system but also showed how dissipation capacity of SMAs could be exploited to change the dynamical behavior of the system. Although SMA systems can be related to complex behaviors, the possibility to change the response with temperature variations is attractive [31].

This contribution deals with the numerical investigation of smart rotordynamics considering an archetypal system composed of a Jeffcot model with SMA elements providing restitution forces on the support. The main motivation is to exploit the remarkable properties of SMAs to avoid undesirable behaviors of the rotor–bearing system. Furthermore, temperature dependence of SMA elements offers an adaptive-passive possibility for control purposes that can be easily implemented avoiding some complex dynamics related to elastic supports. The main goal of this paper is to establish a qualitative comparison between linear elastic and SMA supports, showing the potential application of SMAs to promote vibration reduction. Thermomechanical behavior of SMAs is described through the constitutive model proposed by Paiva et al. [32] that covers the main phenomenological behaviors of SMAs and presents good agreement with experimental data. This contribution shows the feasibility of the use of SMAs to alter dynamical behavior of rotordynamic systems by exploiting two main aspects: dissipation capacity associated with hysteretic behavior during impact; and adaptive behavior related to temperature dependence.

2. Mathematical modeling

This section presents the mathematical model employed to describe the dynamical behavior of the nonsmooth rotordynamic system with SMA element. The system consists of a two-dimensional Jeffcott rotor with mass M, excited by an unbalanced rotating mass m, identified by a fixed distance ρ from the geometrical center of the rotor, as presented in Fig. 1a. During operation, the rotor has intermittent contact with the bearing and it is assumed that contact is non-impulsive and that the friction is neglected. The equivalent stiffness of the rotor is assumed to be k in both directions x and y. System dynamics has two different modes related to contact and non-contact behaviors. Both situations can be evaluated by comparing the radial displacement R of the center of mass of the rotor and the gap γ between the rotor and the bearing: contact ($R \geq \gamma$); and non-contact behavior ($R < \gamma$). During contact, the system presents restitution forces provided by the support elements. Here, two different systems are investigated: linear elastic support and SMA support. All dissipations different from the SMA element hysteretic dissipation are neglected. Fig. 1b shows a disturbed condition where there is contact between the rotor and the bearing; O represents the geometrical center of both the bearing and the rotor in the equilibrium position, while O' is associated with the center of the rotor, taking into account the radial displacement R of the center of mass of the rotor. Two reference frames are adopted—the first one denoted by (x, y) is inertial, while the second one (x', y') is a mobile one attached to the rotor and undergoes only translation in the (x, y) plane to take into account the displacement of the center of mass of the rotor.

Note that ϕ is the initial phase angle, Ω is the angular frequency of the rotor and ψ assigns the angle that the direction of the radial displacement of the rotor makes with the horizontal direction. Besides, $R_x = u(t)$ and $R_y = v(t)$ are the horizontal and vertical displacements of the center of the rotor mass, respectively. Thus, according to Fig. 1b, the system

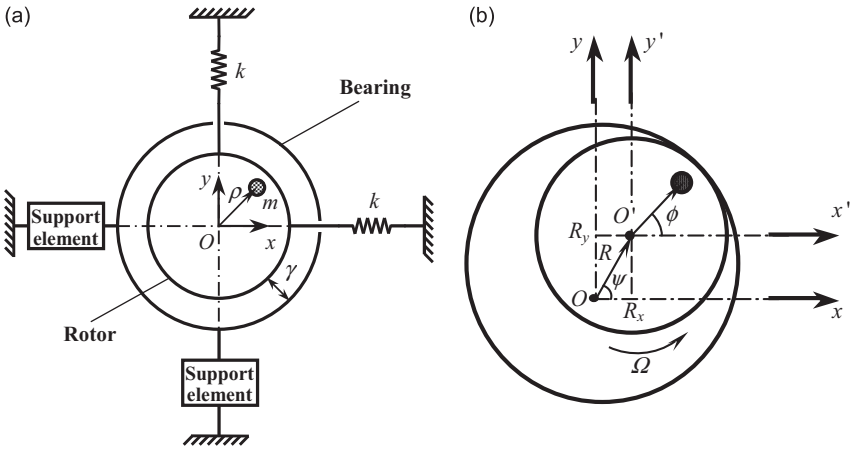

Fig. 1. Physical model for the rotor–bearing system. (a) Equilibrium position; (b) disturbed condition.

must respect the following geometrical conditions:

$$R=\sqrt{u^2+v^2} \quad \cos(\psi)=\frac{u}{R} \quad \sin(\psi)=\frac{v}{R} \tag{1}$$

Fig. 2 presents the free-body diagram for the non-contact and contact situations. F_x and F_y correspond to the linear restitution force acting on the rotor for horizontal and vertical directions, respectively; $\overline{F}_x$ and $\overline{F}_y$ are contact forces, associated with the support element restitution force; F_c is the force due to the unbalanced mass m.

Based on this conceptual model, Newton's second law for both x' and y' directions is employed to establish the following equations of motions [33,34]:

$$\begin{aligned} -F_x-\overline{F}_x+F_c\ \cos(\Omega t+\varphi)&=M\ddot{u}\\ -F_y-\overline{F}_y+F_c\ \sin(\Omega t+\varphi)&=M\ddot{v}\end{aligned} \tag{2}$$

The rotor restitution forces F_x and F_y are assumed to be linear elastic as follows:

$$\begin{aligned} F_x&=ku\\ F_y&=kv\end{aligned} \tag{3}$$

The unbalanced force is given by: $F_c=m\rho\Omega^2$. Moreover, it is important to identify both contact and non-contact situations of the system. Two different support elements are of concern: linear elastic and SMA element. The description of each support depends on the constitutive modeling of the restitution force. By assuming a linear elastic support, the support element restitution forces $\overline{F}_x$ and $\overline{F}_y$, are given by:

$$\begin{aligned} \overline{F}_x&=\begin{cases} k_s\overline{u} & \text{if} \quad R\geq\gamma\\ 0 & \text{if} \quad R<\gamma\end{cases}\\ \overline{F}_y&=\begin{cases} k_s\overline{v} & \text{if} \quad R\geq\gamma\\ 0 & \text{if} \quad R<\gamma\end{cases}\end{aligned} \tag{4}$$

Note that $(R-\gamma)$ is the radial displacement of the bearing. Thus, $\overline{u}=(R-\gamma)\cos(\psi)$ and $\overline{v}=(R-\gamma)\sin(\psi)$ are the support displacements on the horizontal and vertical directions, respectively, while k_s is the support stiffness.

The SMA support element employed in the bearing may be designed as a spring or a beam structure; though, the SMA element is evaluated as an equivalent bar of cross sectional area A and length l subjected to tension/compression that would correspond to an SMA element. Therefore, the forces $\overline{F}_x$ and $\overline{F}_y$ provided by the SMA supports are defined as follows:

$$\begin{aligned} \overline{F}_x&=\begin{cases} \sigma_x A & \text{if} \quad R\geq\gamma\\ 0 & \text{if} \quad R<\gamma\end{cases}\\ \overline{F}_y&=\begin{cases} \sigma_y\ A & \text{if} \quad R\geq\gamma\\ 0 & \text{if} \quad R<\gamma\end{cases}\end{aligned} \tag{5}$$

where σ_x and σ_y are the uniaxial stresses developed in the SMA element for the horizontal and vertical directions, respectively. Accordingly, the SMA element deformation can be evaluated as:

$$\begin{aligned} \varepsilon_x&=\frac{\overline{u}}{l}=\frac{(R-\gamma)\ \cos(\psi)}{l}\\ \varepsilon_y&=\frac{\overline{v}}{l}=\frac{(R-\gamma)\ \sin(\psi)}{l}\end{aligned} \tag{6}$$

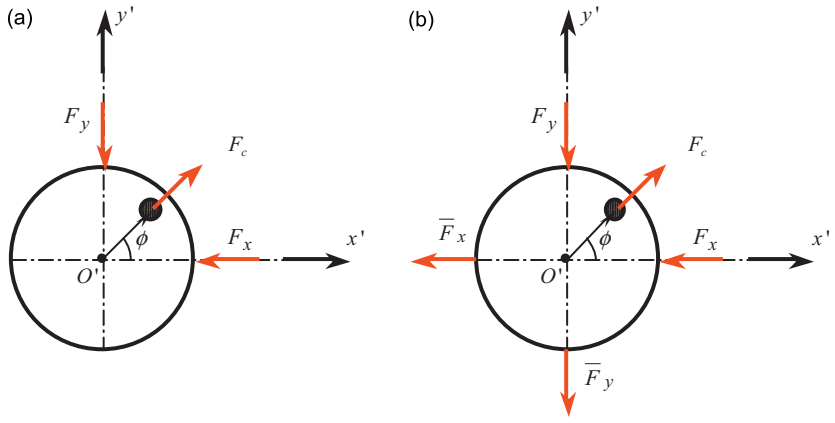

Fig. 2. Free-body diagram for the rotor–bearing system, (a) non-contact situation; (b) contact situation.

Finally, it is possible to rewrite the equations of motion (Eq. (2)) in their final form for both directions as:

$$M\ddot{u}+ku+\overline{F}_x = m\rho\Omega^2\cos(\Omega t+\varphi)$$
$$M\ddot{v}+kv+\overline{F}_y = m\rho\Omega^2\sin(\Omega t+\varphi) \tag{7}$$

where $\overline{F}_x$ and $\overline{F}_y$ may be evaluated according to either Eq. (4) for a linear elastic support on the bearing or Eq. (5) for an SMA support. The next section presents the constitutive modeling related to the thermomechanical behavior of the SMA. This equations provides a proper description of the forces $\overline{F}_x$ and $\overline{F}_y$.

2.1. Constitutive modeling

This section deals with the constitutive modeling of the thermomechanical behavior of the SMA element. There are several theories capable to perform the macroscopic description of the main phenomena presented by SMA materials [35,36]. Here, a simplification of the model proposed by Paiva et al. [32] is employed [37,38]. This simplified version considers a one-dimensional model with four macroscopic phases, being able to describe the main SMA behaviors such as: pseudoelasticity, shape memory effect, phase transformation induced by temperature variation and internal sub-loops due to incomplete phase transformations. The constitutive equations of this model establish the stress σ as a function of the observable variables strain ε and temperature T; besides, three internal variables that correspond the volume fraction of each phase: β_1 and β_2 are the volume fractions associated with the detwinned martensitic variants, respectively, related to tension (denoted by $M+$) and compression (denoted by $M-$) behaviors, while β_3 is the volume fraction associated with austenitic phase (denoted by A). Note that a fourth phase related to twinned martensite is also considered in the formulation but, as a matter of fact, it may be written as function of the other three by the relation: $\beta_4=1-\beta_1-\beta_2-\beta_3$. Therefore, the following set of constitutive equations is defined:

$$\sigma = E\varepsilon+[\alpha+E\alpha_h](\beta_2-\beta_1)-\Theta\,(T-T_0) \tag{8}$$

$$\dot{\beta}_1 = \frac{1}{\eta_1}\left\{\alpha\varepsilon+\Lambda+\left[2\alpha_h\alpha+E\alpha_h^2\right](\beta_2-\beta_1)+\alpha_h[E\varepsilon-\Theta\,(T-T_0)]-\partial_{\beta_1}J_\pi\right\}+\partial_{\dot{\beta}_1}J_\chi \tag{9}$$

$$\dot{\beta}_2 = \frac{1}{\eta_2}\left\{-\alpha\varepsilon+\Lambda-\left[2\alpha_h\alpha+E\alpha_h^2\right](\beta_2-\beta_1)-\alpha_h[E\ \varepsilon-\Theta\,(T-T_0)]-\partial_{\beta_2}J_\pi\right\}+\partial_{\dot{\beta}_2}J_\chi \tag{10}$$

$$\dot{\beta}_3 = \frac{1}{\eta_3}\left\{-\frac{1}{2}\,(E_A-E_M)\,[\varepsilon+\alpha_h(\beta_2-\beta_1)]^2+\Lambda_3+(\Theta_A-\Theta_M)\,\,(T-T_0)\,\left[\varepsilon+\alpha_h(\beta_2-\beta_1)\right]-\partial_{\beta_3}-J_\pi\right\}+\partial_{\dot{\beta}_3}J_\chi \tag{11}$$

In these equations, $E=E_M+\beta_3(E_A-E_M)$ is the elastic modulus, $\Theta=\Theta_M+\beta_3(\Theta_A-\Theta_M)$ is related to the coefficient of thermal expansion, while T_0 is a reference temperature. The subscript indices "M" and "A" refer to martensitic and austenitic phases, respectively. The parameter α is related to the height of the hysteresis loop, while α_h is related to its width. The terms $\partial_{\beta_n}\,J_\pi\,(n=1,2,3)$ are the sub-differential of the indicator function J_π with respect to $\beta_n(n=1,2,3)$, being related to the internal constrains related to the coexistence of phases.

The terms $\partial_{\dot{\beta}_n}J_\chi\,(n=1,2,3)$ are sub-differentials of the indicator function J_χ with respect to $\dot{\beta}_n(n=1,2,3)$, which is associated with the conditions for the proper description of internal sub-loops due to incomplete phase transformations. These restrictions also avoid the physically unfeasible transformations: $M+\Rightarrow M$ and $M-\Rightarrow M$.

The parameters $\Lambda=\Lambda(T)$ and $\Lambda_3=\Lambda_3(T)$ are associated with critical stress values for phase transformations, being defined as follows:

$$\Lambda = \begin{cases} -L_0+\frac{L}{T_M}\,(T-T_M) & \text{if } T>T_M \\ -L_0 & \text{if } T\le T_M \end{cases} \tag{12}$$

$$\Lambda_3 = \begin{cases} -L_0^A+\frac{L^A}{T_M}\,(T-T_M) & \text{if } T>T_M \\ -L_0^A & \text{if } T\le T_M \end{cases} \tag{13}$$

where T_M is the temperature below which the martensitic phase is stable, while L_0, L, L_0^A and L^A are parameters that control phase transformations.

In order to consider different characteristics of phase transformation kinetics, the dissipation parameter $\eta_n(n=1,2,3)$ may assume different values for loading and unloading behaviors.

For further details, please see Ref. [32]. The use of constitutive Eqs. (8)–(11) in the equations of motion of the rotordynamical system allows the description of the restoring forces $\overline{F}_x$ and $\overline{F}_y$ on the SMA support element.

3. Numerical simulations

This section presents numerical simulations of the rotor–bearing system with SMA supports, exploring the pseudoelastic behavior. The main goal of the present analysis is to compare the SMA dynamical system behavior with

Table 1
SMA properties.

E_A (GPa)	E_M (GPa)	α (MPa)	α_h (MPa)
54	42	50	50
L_0 (MPa)	L (MPa)	L_0^A (MPa)	L^A (MPa)
0.15	4.0	6.3	165
Θ_A (MPa/K)	Θ_M (MPa/K)	T_M (K)	T_0 (K)
0.74	0.17	201.4	298.0
η_1 (MPa s)	η_2 (MPa s)	η_3 (MPa s)	
5.0	5.0	2.0	

Table 2
Rotor–bearing system parameters.

M (kg)	m (kg)	γ (m)	ρ (m)	k (N/m)
15	0.15	0.002	0.055	3.92

Table 3
Geometric data of an equivalent spring related to the SMA element.

D (m)	d (m)	N	d_{shaft} (m)	J_P (m^4)
0.008	0.0003	10	0.01	9.81×10^{-10}

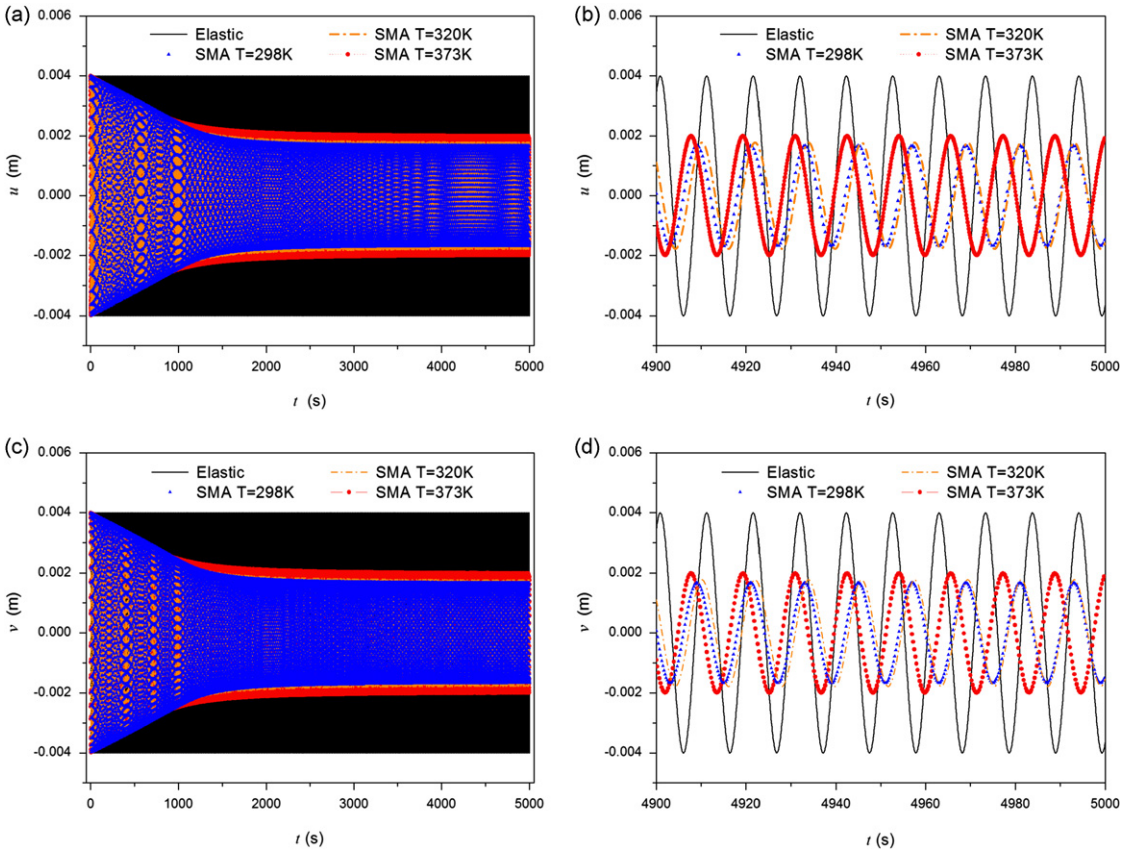

Fig. 3. Displacement evolution. (a) x-direction; (b) steady state in x-direction; (c) y-direction; (d) steady state in y-direction.

the one with elastic support, highlighting their differences. This approach allows one to obtain a general qualitative comprehension about the rotor system dynamics, defining some potential situations where SMA employment may avoid undesirable behaviors for control purposes.

The constitutive properties of the SMA element are presented in Table 1. Table 2 presents the rotor–bearing parameters. Both sets of parameters apply for all simulations throughout the paper, as well as the velocity initial conditions ($\dot{u}_0 = \dot{v}_0 = 0$). All other information is addressed during each specific simulation.

In order to furnish a better comprehension of the restitution force provided by the SMA element, Table 3 presents the data of an equivalent spring that would correspond to the SMA bar presenting the same stiffness according to the constitutive parameters of Table 1. In Table 3, D represents the diameter of the SMA spring, d represents the wire diameter, N is the number of active coils, d_{shaft} represents the shaft diameter that helps the estimation of the equivalent stiffness for the bearing support and J_P represents the area moment of inertia. These parameters provide an equivalent stiffness $k_s = 2.867$ N/m for the SMA element in the austenitic phase.

3.1. Free vibration

This section deals with the free vibration analysis of the rotor system and its main goal is to observe the general thermomechanical behavior of the SMA element promoting the model verification. This simulation is performed without the external excitation, vanishing the unbalanced mass ($m = 0$ kg). Furthermore, it is assumed initial conditions in such a way that the offset for both directions must be greater than the gap between the rotor and bearing ($u_0 = v_0 = 0.004$ m), ensuring contact.

Basically, the free vibration analysis establishes a comparison between two different systems: elastic and SMA supports. Concerning the SMA system, three different temperatures are investigated: $T = 298$ K; $T = 320$ K and $T = 373$ K. The change in temperature alters the position of the hysteresis loop in the force–displacement space, changing the amount of dissipated energy. This analysis illustrates the adaptive behavior of SMA system related to temperature dependence.

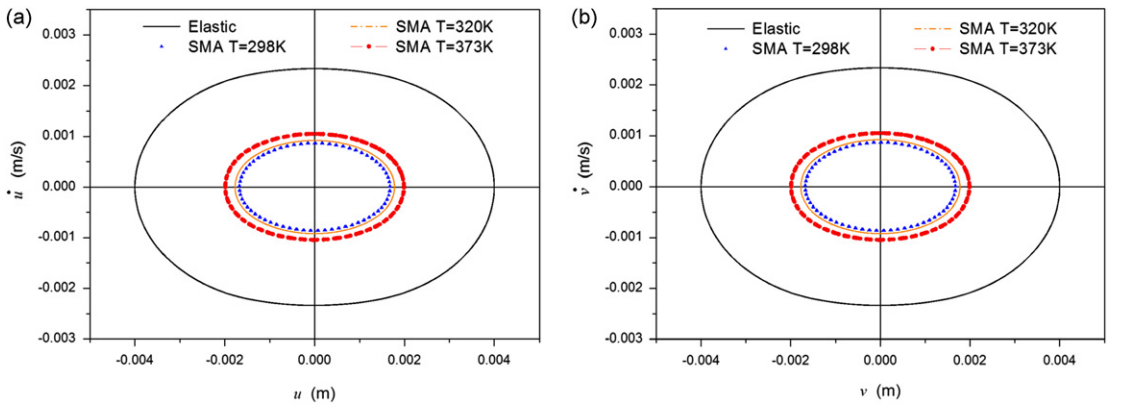

Fig. 4. Phase space orbits. (a)$u \times \dot{u}$; (b) $v \times \dot{v}$.

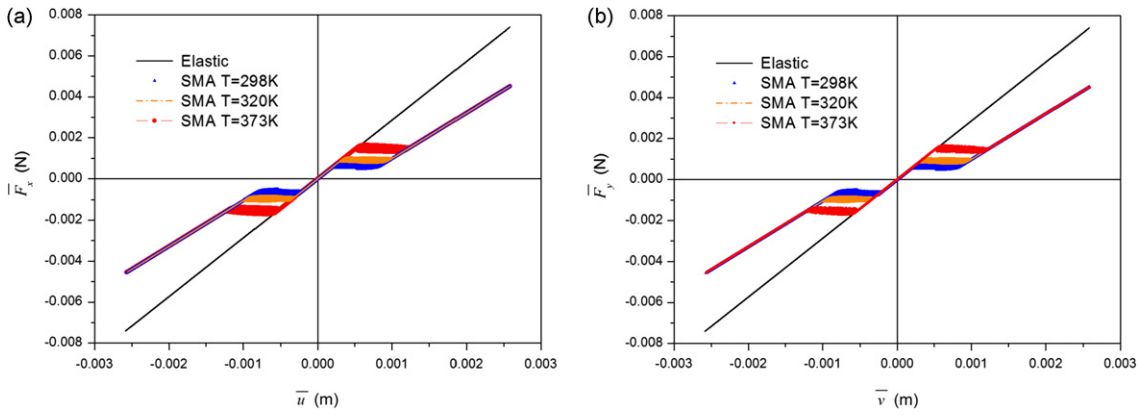

Fig. 5. Force–displacement curves for the support element. (a) x-direction; (b) y-direction.

Fig. 3 shows the time history of horizontal (u) and vertical (v) rotor displacement for these four situations (elastic compared with three different SMA temperatures). It is noticeable that, for the SMA system, there is a transient where the displacement amplitude decays until the steady state is reached. This transient is related to hysteretic dissipation of the SMA element, while the steady state is associated with its elastic response. Fig. 3b and d highlight the time-response showing the differences in the amplitude of the steady state movement. Phase space plots of the steady state responses are shown in Fig. 4.

The hysteretic behavior of the SMA element is now observed through the force–displacement diagrams showed in Fig. 5, for x and y directions. It is worthwhile to observe that the displacements, u and v, in Figs. 3 and 4 refer to the rotor

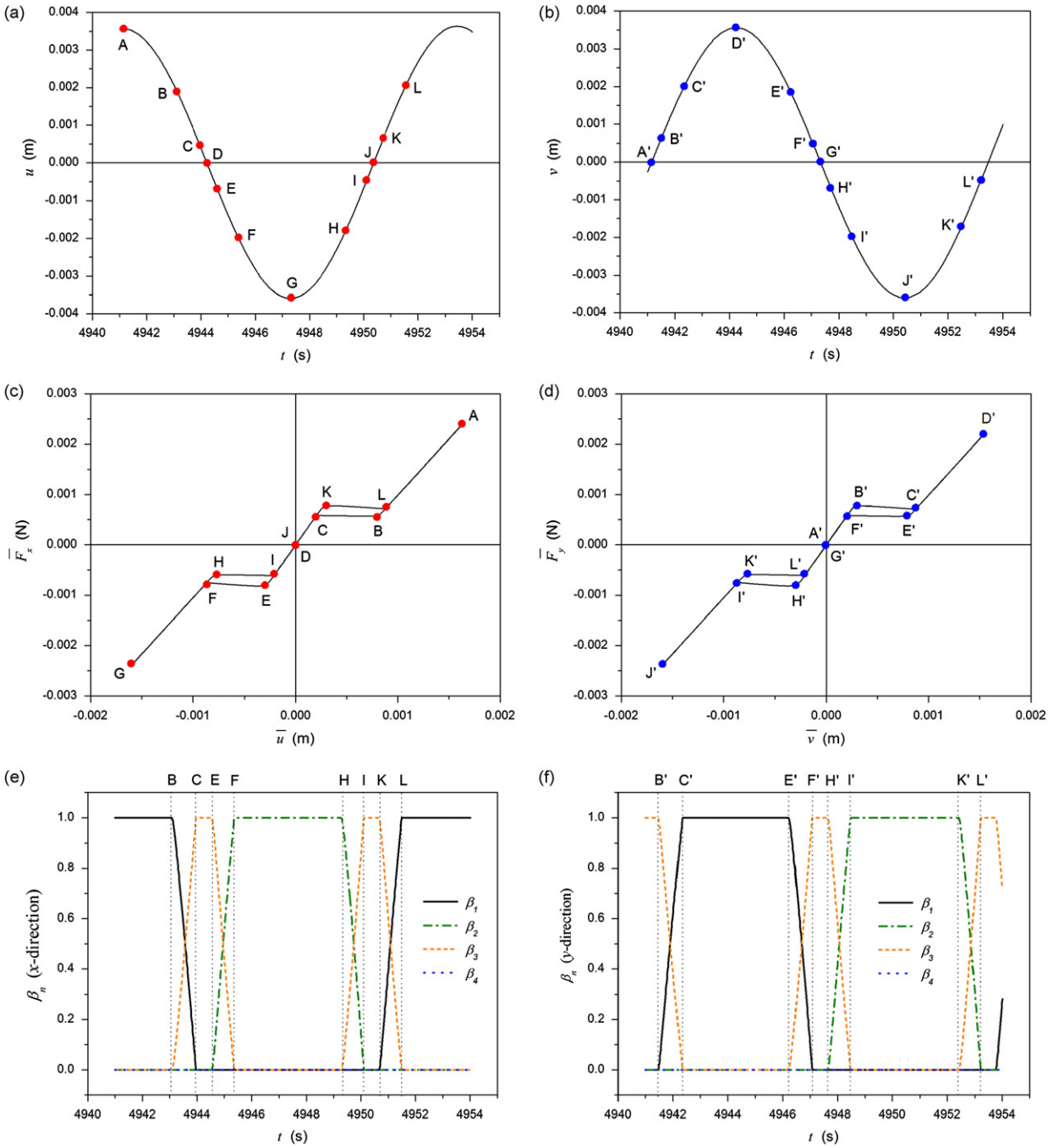

Fig. 6. Phase transformation analysis. (a) Displacement evolution for x-direction; (b) displacement evolution for y-direction; (c) force–displacement diagram for x-direction; (d) force–displacement diagram for y-direction; (e) volume fractions evolution for x-direction; (f) volume fractions evolution for y-direction.

displacement, while, in Fig. 5, $\overline{u}$ and $\overline{v}$ are related to the displacement of the bearing support. Note that temperature variation promotes a change in the position of the hysteresis loop, and the increase in temperature increases the distance from the horizontal axis with null force. Therefore, this temperature variation changes the energy dissipation related to the hysteretic response.

3.2. Forced vibration

This section deals with numerical simulations of the forced response of the rotor–bearing system with SMA supports. Three situations are treated: the first one evaluates the system behavior highlighting phase transformation evolution; the second one emphasizes the SMA temperature influence on system dynamics; finally, the third one discusses the SMA potential to perform dynamical changes in rotor systems.

For the first case, consider the following parameters: $T=298$ K; $m=0.15$ kg; $\Omega=0.5112$ rad/s; $\phi=0$ rad and $u_0=v_0=0.0001$ m as initial conditions. After a transient response, steady state is reached and Fig. 6 highlights the system behavior establishing the relation among displacements, forces and volume fractions. Fig. 6a and b present one cycle of the steady state displacement response in both x and y directions. Fig. 6c and d show force–displacement curves of the SMA support elements for directions x and y. Fig. 6e and f show the time history of the volume fractions of the macroscopic phases. Note that some time instants are highlighted with letters, allowing the analysis of the evolution of each variable for the whole dynamical process.

Considering the x-direction (Fig. 6a, c and e), the initial state is represented by the point A, where the SMA element is in detwinned martensite state (variant $M+$). From point A to point B, the system presents an elastic recovery according to phase $M+$. Between the points B and C, the SMA undergoes a reverse transformation ($M+ \Rightarrow A$), such that, in point C ($t \cong 4943{,}96$ s), the structure is totally austenitic. After that, the system presents an elastic response according to phase A passing through point D (where there is no displacement) towards point E ($t \cong 4944{,}59$ s), where it starts an $A \Rightarrow M-$ martensitic transformation (between points E and F). From point F on ($t \cong 4945{,}37$ s), the SMA support presents an elastic response according to phase $M-$, until it reaches the maximum negative point G. Afterward, from point G to point H ($t \cong 4949{,}34$ s), another elastic recovery according to phase $M-$ occurs. Between the points H and I, the SMA element

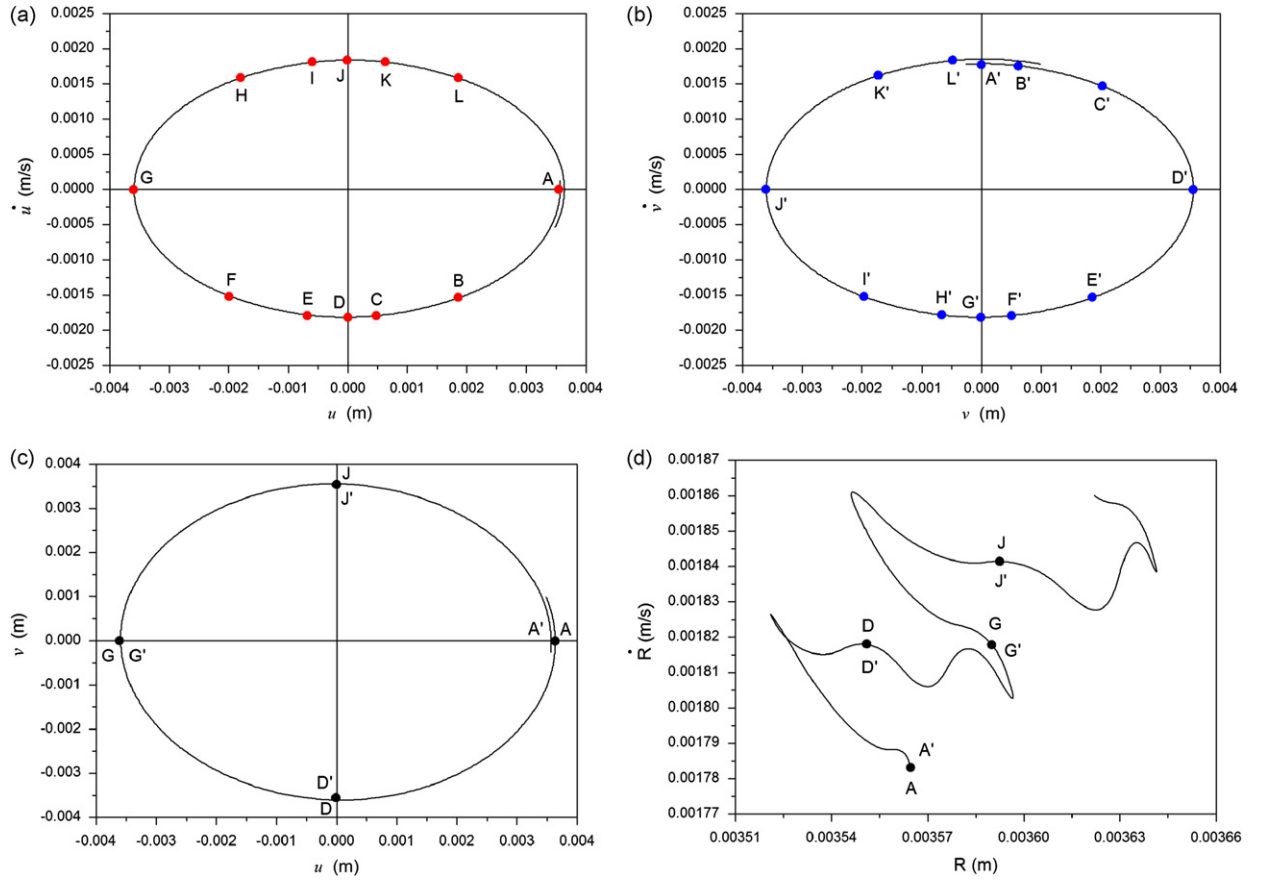

Fig. 7. Phase space orbits. (a) $u \times \dot{u}$; (b) $v \times \dot{v}$; (c) $u \times v$; (d) $R \times \dot{R}$.

undergoes another reverse transformation ($M- \Rightarrow A$), such that, in point I ($t \cong 4950{,}04$ s), the structure is again totally austenitic. Then, there is a new elastic response according to phase A, passing again through point J (where there is no displacement), until it reaches point K, where it starts another martensitic transformation ($A \Rightarrow M+$) that lasts until point L. At this point, the SMA structure is fully $M+$ again and, from this point on, there is an elastic response according to phase $M+$, completing the cycle. A similar analysis can be done by considering the y-direction (Fig. 6b, d and f). It is interesting to note that the displacements in x and y directions are not synchronized (as they are in the simulation for free vibrations).

Fig. 7 shows the phase space orbits for the same situation, highlighting the same points. Fig. 7a and b show the orbits $u \times \dot{u}$ and $v \times \dot{v}$, respectively. These orbits show that the system oscillates around the equilibrium points: $(u,\dot{u}) = (0,0)$ and $(v,\dot{v}) = (0,0)$. Fig. 7c shows the phase space that represents the center of the rotor displacement, taking into account that the rotor touches the bearing during the spin trajectory. Fig. 7d shows the behavior of rotor radial trajectory. This trajectory is represented by R and shows the behavior in terms of the center of the rotor displacement. Both Fig. 7c and d present some noticeable points (A–A′, D–D′, G–G′ and J–J′) that denote the null displacement for either u or v.

At this moment, one considers a simulation with the same parameters of the previous one, i.e., $m=0.15$ kg; $\Omega=0.5112$ rad/s; $\phi=0$ rad and $u_0=v_0=0.0001$ m. A comparison with the case with elastic support is now in focus for different temperatures of the SMA element. The SMA system can exploit temperature variation to avoid undesirable behaviors. This temperature dependence is related to an adaptive characteristic of the SMA system that can be used for control purposes. In order to illustrate such capacity, consider a situation where the system presents the beating phenomenon by assuming that the rotor–bearing system is excited by a frequency close to the system natural frequency.

The developed analysis establishes a comparison among three different cases: elastic system and SMA system with two distinct temperatures ($T=298$ K and $T=493$ K). Fig. 8 presents displacement time history, while Fig. 9 shows the same responses in the form of steady state phase space orbits ($u \times v$) and the respective time history of R. Fig. 10 presents the

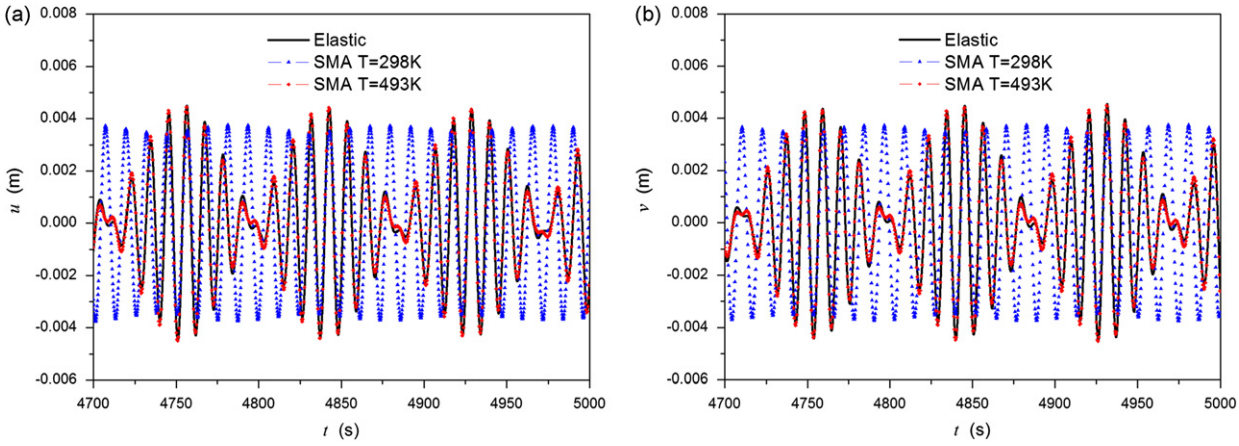

Fig. 8. Displacement evolution. (a) x-direction; (b) y-direction.

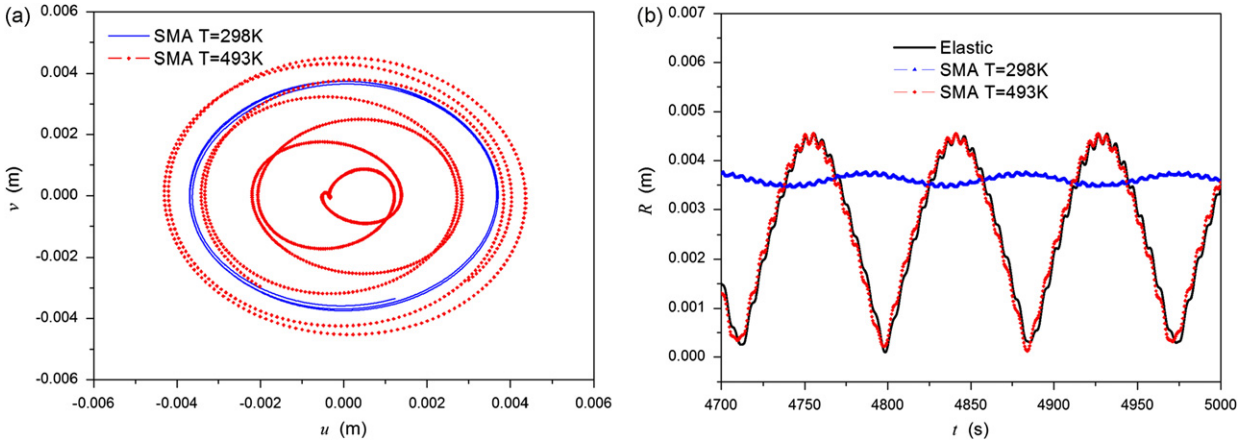

Fig. 9. (a) Phase space orbits $u \times v$, (b) radial displacement evolution.

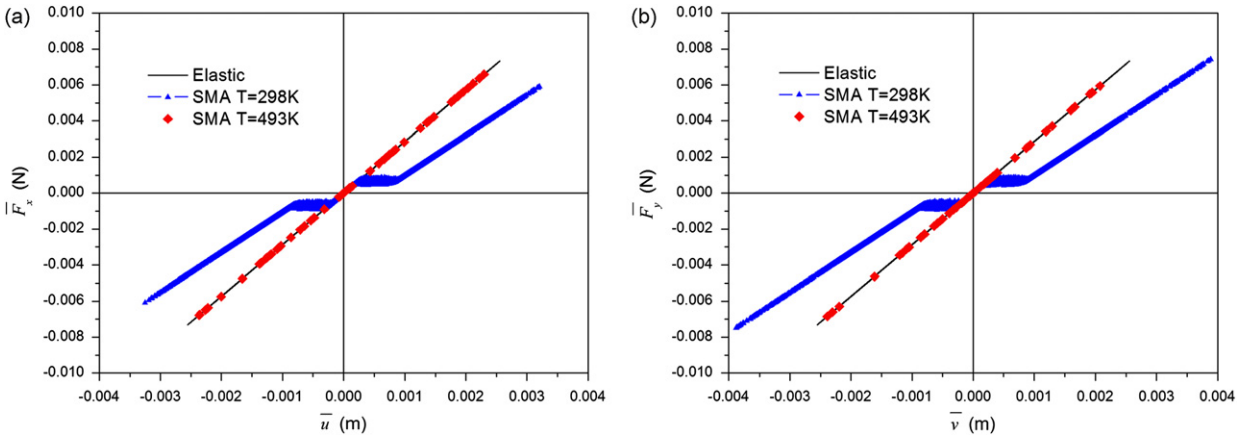

Fig. 10. Force–displacement curves. (a) *x*-direction; (b) *y*-direction.

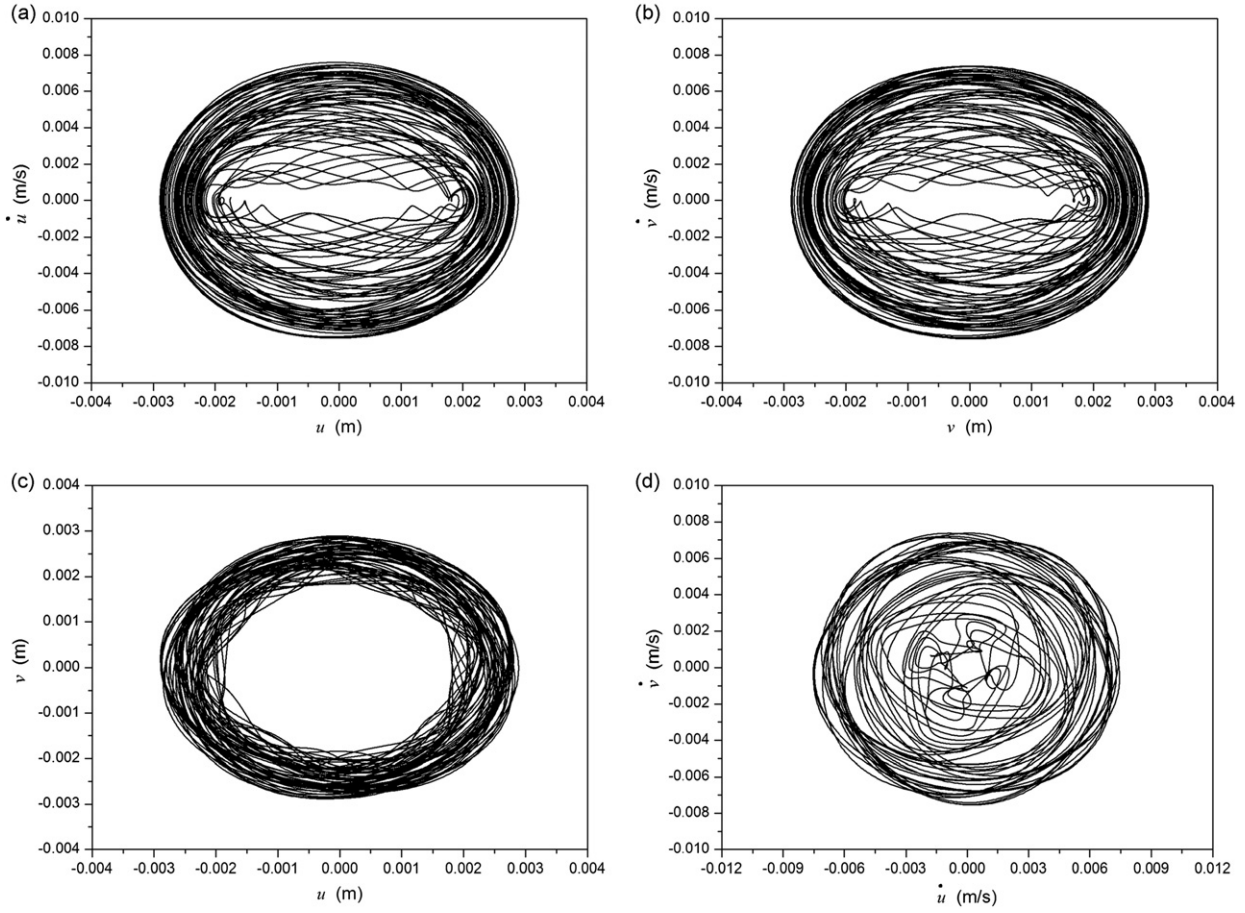

Fig. 11. Phase space orbits for the system with elastic element. (a) $u \times \dot{u}$; (b) $v \times \dot{v}$; (c) $u \times v$; (d) $\dot{u} \times \dot{v}$.

force–displacement curves associated with these responses. According to them, the higher temperature behavior (T=493 K) is related to a situation where the SMA element does not present phase transformation; thus, its response is likewise the elastic system. Nevertheless, for a lower temperature (T=298 K), there is a change in the response and the beating does not occur anymore. The hysteretic behavior is responsible for this change.

The nonlinear dynamical behavior of the rotor–bearing system is very rich, presenting periodic, quasi-periodic and chaotic responses. From now on, the interest is to evaluate if the SMA support is able to avoid some undesirable responses. Therefore, consider a situation where the elastic system presents a chaotic response by assuming the following parameters: $T=298$ K; $m=0.15$ kg; $k_s=350$ N/m; $\Omega=1.8$ rad/s; $\phi=0$ rad and $u_0=v_0=0.001$ m.

Fig. 11 shows the elastic system response by presenting the phase space. It is noticeable the chaotic-like response of the system. Fig. 12, as well, suggests this chaotic behavior by evaluating the initial conditions sensitivity. Note that two different but very close initial conditions cause, after some time, completely different responses.

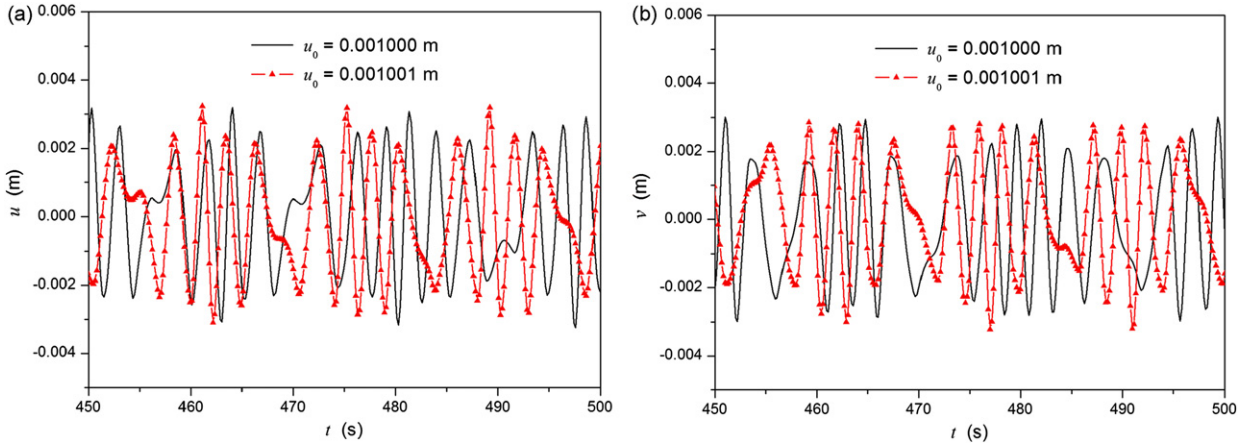

Fig. 12. Initial conditions sensitivity. Displacement evolution for x-direction; (b) displacement evolution for y-direction.

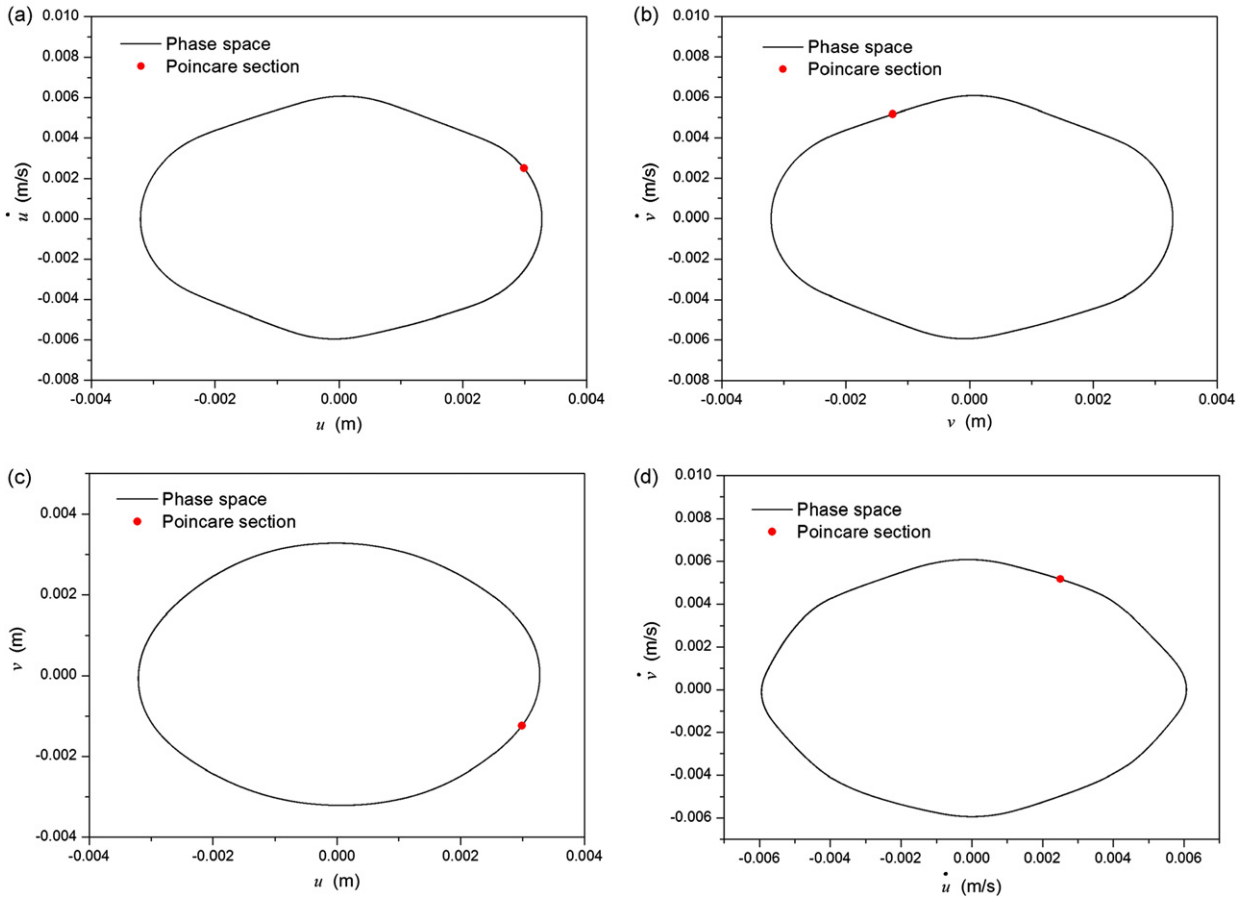

Fig. 13. Phase space orbits and Poincare section for the system with SMA element. (a) $u\times\dot{u}$; (b) $v\times\dot{v}$; (c) $u\times v$; (d) $\dot{u}\times\dot{v}$.

The inclusion of the SMA element can change this kind of behavior. Fig. 13 shows the phase space and the Poincare section for the system with SMA elements. Through these diagrams, it can be observed that the use of SMA elements changes the system response to a period-1 behavior. Therefore, the hysteretic behavior of the SMA element can dramatically change the system response.

Fig. 14 compares the time evolution of displacement and velocity for both systems. Once again it is possible to compare the chaotic-like response of the elastic system with the period-1 response of the SMA system.

In order to assure that chaotic-like response of the elastic system is really chaotic, frequency analysis is focused on for both systems. Fig. 15 shows the frequency spectrum of each system for each direction. Note that the energy is spread over

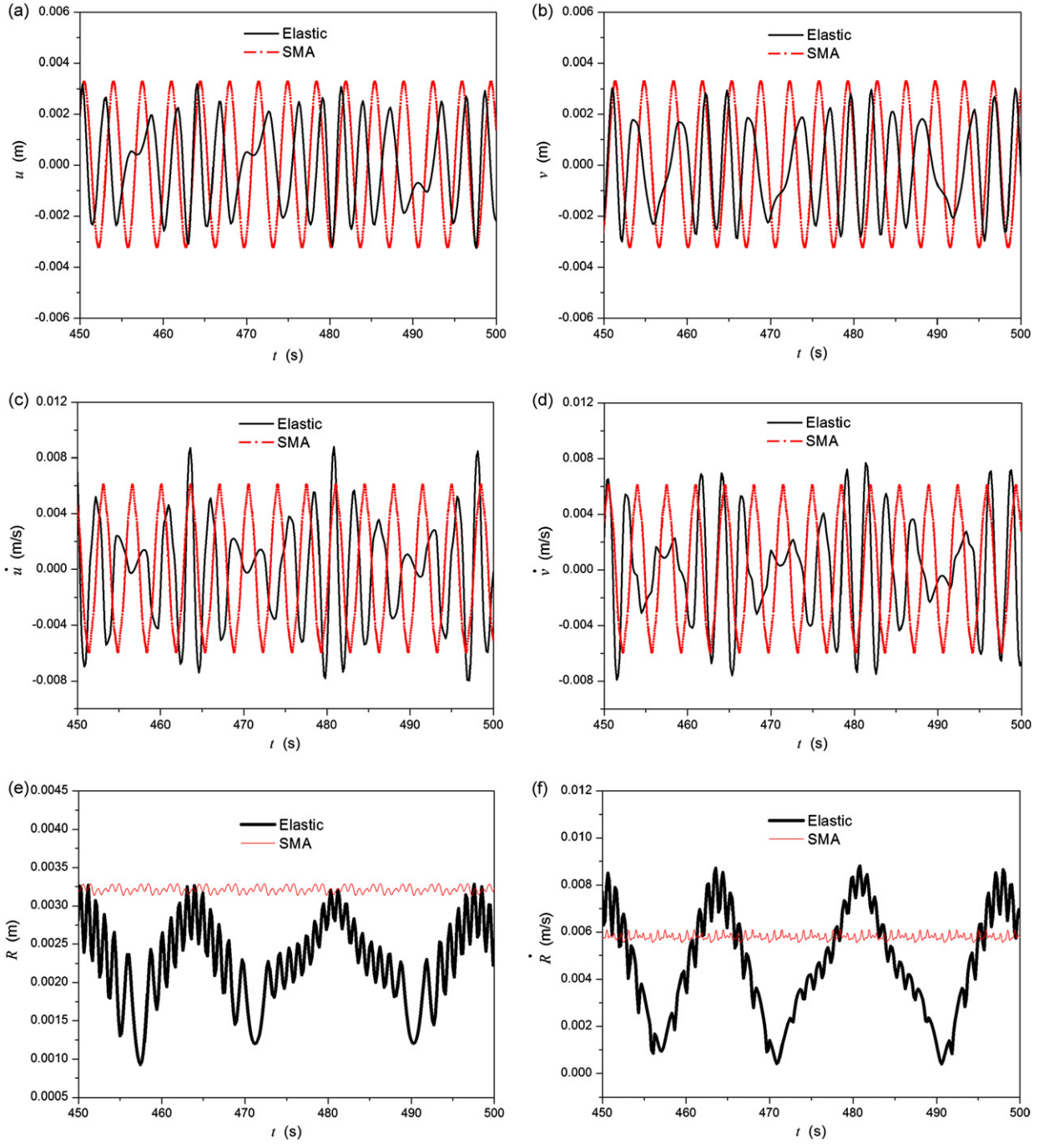

Fig. 14. Time evolutions for chaotic elastic motion and period-1 SMA motion. (a) Displacement for *x*-direction; (b) displacement for *y*-direction; (c) velocity for *x*-direction; (d) velocity for *y*-direction; (e) displacement for radial direction; (f) velocity for radial direction.

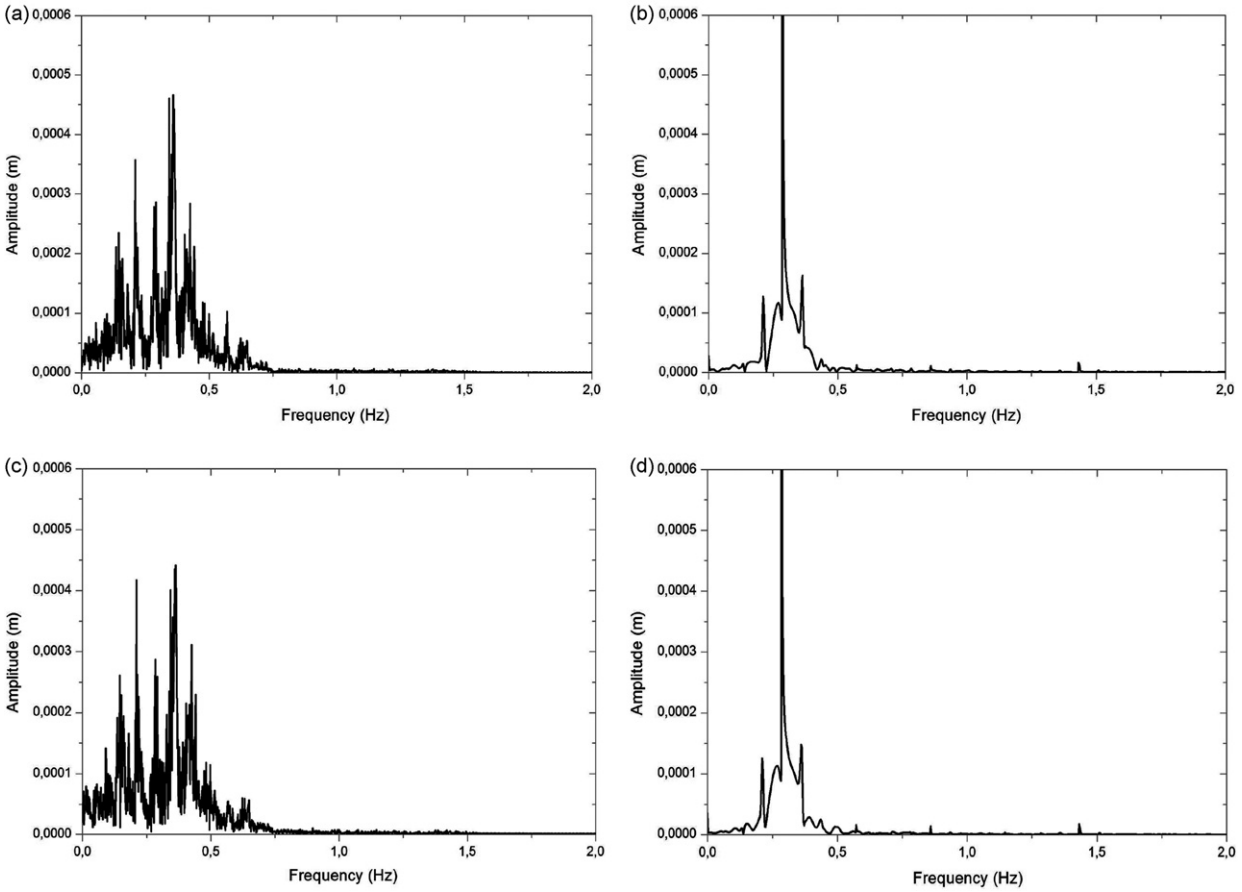

Fig. 15. Frequency spectra. (a) Elastic system in *x*-direction; (b) SMA system in *x*-direction; (c) elastic system in *y*-direction; (d) SMA system in *y*-direction.

a range for the chaotic elastic signal while it is restrict to a main discrete frequency for the SMA periodic response. This analysis confirms the possibility of the use of SMA elements to avoid undesirable responses of rotordynamical systems.

4. Conclusions

This work presents the nonlinear dynamical analysis of a Jeffcott rotor system, considering a shape memory alloy restitution element on the bearing support. The mathematical model introduces the SMA constitutive equations into the well-known Jeffcott dynamic formulation. Numerical simulations are conducted in order to establish a qualitative comparison between elastic and SMA systems, emphasizing the intrinsic dissipation due to hysteretic behavior of the SMA response and temperature dependent behavior. Initially, free vibration analysis is carried out for the model verification. This behavior attests the amplitude decay, related to hysteretic dissipation of the SMA element, leading to a steady state response associated with its austenitic elastic behavior. The forced vibration is then focused on, showing that SMAs can be used not only to reduce vibration amplitudes due to their intrinsic dissipation, but also to change the system dynamics. Moreover, SMA offers different possibilities for control purposes. Passive control can be exploited substituting an elastic support that produces undesirable responses for an SMA element. Temperature dependence of the SMA element can be exploited in order to develop passive-adaptive control since temperature variations can change the qualitative dynamic pattern.

Acknowledgements

The authors would like to acknowledge the support of the Brazilian Research Agencies CNPq, CAPES and FAPERJ and through the INCT-EIE (National Institute of Science and Technology—Smart Structures in Engineering) the CNPq and FAPEMIG. The acknowledgement applies also to Air Force Office of Scientific Research (AFOSR).

References

[1] Y. Zhang, B. Wen, A. Leung, Reliability analysis for rotor rubbing, *Journal of Vibration and Acoustics* 124 (1) (2002) 58–62.
[2] B. Schweizer, M. Sievert, Nonlinear oscillations of automotive turbocharger turbines, *Journal of Sound and Vibration* 321 (3–5) (2009) 955–975.
[3] S.K. Laha, Nonlinear dynamic analysis of a flexible rotor supported on porous oil journal bearing, *Communications in Nonlinear Science and Numerical Simulation* 16 (2011) 1617–1631.
[4] G.N.D. Sudhakar, A.S. Sekhar, Identification of unbalance in a rotor bearing system, *Journal of Sound and Vibration* 330 (2011) 2299–2313.
[5] P.S. Keogh, Contact dynamic phenomena in rotating machines: active/passive considerations, *Mechanical Systems and Signal Processing* 29 (2012) 19–33.
[6] H.H. Jeffcott, The lateral vibration of loaded shifts in the neighborhood of a whirling speed—the effects of want of balance, *Philosophical Magazine Series* 6 (37) (1919) 304–314.
[7] E.V. Karpenko, M. Wiercigroch, M.P. Cartmell, Regular and chaotic dynamics of a discontinuously nonlinear rotor system, Chaos, Solitons and Fractals, 13, 6, 1231–1242.
[8] E.E. Pavlovskaia, E.V. Karpenko, M. Wiercigroch, Nonlinear dynamics of a Jeffcott rotor with a preloaded snubber ring, *Journal of Sound and Vibration* 276 (1–2) (2004) 361–379.
[9] E.V. Karpenko, M. Wiercigroch, E.E. Pavlovskaia, R.D. Neilson, Experimental verification of Jeffcott rotor model with preloaded snubber ring, *Journal of Sound and Vibration* 298 (4–5) (2006) 907–917.
[10] Z. Shang, J. Jiang, L. Hong, The global responses characteristics of a rotor/stator rubbing system with dry friction effects, *Journal of Sound and Vibration* 330 (10) (2011) 2150–2160.
[11] J. Warminski, G. Litak, M.P. Cartmell, R. Khanin, M. Wiercigroch, Approximate analytical solutions for primary chatter in the nonlinear metal cutting model, *Journal of Sound and Vibration* 259 (4) (2003) 917–933.
[12] L.F.P. Franca, H.I. Weber, Experimental and numerical study of a new resonance hammer drilling model with drift, *Chaos, Solitons and Fractals* 21 (2004) 789–801.
[13] M. Wiercigroch, J. Wojewoda, A.M. Krivtsov, Dynamics of ultrasonic percussive drilling of hard rocks, *Journal of Sound and Vibration* 280 (3-5) (2005) 739–757.
[14] B. Blazejczyk-Okolewska, T. Kapitaniak, Dynamics of impact oscillator with dry friction, *Chaos, Solitons and Fractals* 7 (9) (1996) 1455–1459.
[15] B. Blazejczyk-Okolewska, T. Kapitaniak, Co-existing attractors of impact oscillator, *Chaos, Solitons and Fractals* 9 (8) (1998) 1439–1443.
[16] Y. Maistrenko, T. Kapitaniak, P. Szuminski, Locally and globally riddled basins in two coupled piecewise-linear maps, *Physical Review E* 56 (6) (1997) 6393–6399.
[17] M. Wiercigroch, Modelling of dynamical systems with motion dependent discontinuities, *Chaos, Solitons and Fractals* 11 (2000) 2429–2442.
[18] R.I. Leine, Bifurcations in discontinuous mechanical systems of Filippov-type, Ph.D. Thesis, Technische Universiteit Eindhoven.
[19] S. Divenyi, M.A. Savi, L.F.P. Franca, H.I. Weber, Nonlinear dynamics and chaos in systems with discontinuous support, *Shock and Vibration* 13 (4) (2006) 315–326.
[20] M.A. Savi, S. Divenyi, L.F.P. Franca, H.I. Weber, Numerical and experimental investigations of the nonlinear dynamics and chaos in non-smooth systems, *Journal of Sound and Vibration* 30 (1-2) (2007) 59–73.
[21] M.D. Todd, L.N. Virgin, Natural frequencies considerations of an impact oscillator, *Journal of Sound and Vibration* 194 (3) (1996) 452–460.
[22] M.D. Todd, L.N. Virgin, An experimental impact oscillator, *Chaos, Solitons and Fractals* 8 (4) (1997) 699–714.
[23] K.N. Slade, L.N. Virgin, P.V. Bayly, Extracting information from interimpact intervals in a mechanical oscillator, *Physical Review E* 56 (3) (1997) 3705–3708.
[24] M. Wiercigroch, V.W.T. Sin, K. Li, Measurement of chaotic vibration in a symmetrically piecewise linear oscillator, *Chaos, Solitons and Fractals* 9 (1/2) (1998) 209–220.
[25] M. Wiercigroch, V.W.T. Sin, Experimental study of a symmetrical piecewise base excited oscillator, *Journal of Applied Mechanics—ASME* 65 (1998) 657–663.
[26] C.J. Begley, L.N. Virgin, Impact response and the influence of friction, *Journal of Sound and Vibration* 211 (5) (1998) 801–818.
[27] P.T. Piiroinen, L.N. Virgin, A.R. Champneys, Chaos and period-adding: experimental and numerical verification of the grazing bifurcation, *Journal of Nonlinear Science* 14 (2004) 383–404.
[28] S. Divenyi, M.A. Savi, H.I. Weber, L.F.P. Franca, Experimental investigation of an oscillator with discontinuous support considering different system aspects, *Chaos, Solitons and Fractals* 38 (2008) 685–695.
[29] B.C. Santos, M.A. Savi, Nonlinear dynamics of a nonsmooth shape memory alloy oscillator, *Chaos, Solitons and Fractals* 40 (1) (2009) 197–209.
[30] E. Sitnikova, E. Pavlovskaia, M. Wiercigroch, M.A. Savi, Vibration reduction of the impact system by an SMA restraint: numerical analysis, *International Journal of Nonlinear Mechanics* 45 (9) (2010) 837–849.
[31] M.A. Savi, A.S. de Paula, D.C. Lagoudas, Numerical investigation of an adaptive vibration absorber using shape memory alloys, *Journal of Intelligent Material Systems and Structures* 22 (1) (2011) 67–80.
[32] A. Paiva, M.A. Savi, P.M.C.L. Pacheco, A.M.B. Braga, A constitutive model for shape memory alloys considering tensile–compressive asymmetry and plasticity, *International Journal of Solids and Structures* 42 (2005) 3439–3457.
[33] D.H. Gonsalves, R.D. Neilson, D.S. Barr, A study of response of a discontinuously nonlinear rotor system, *Nonlinear Dynamics* 7 (4) (1995) 451–470.
[34] E.V. Karpenko, M. Wiercigroch, M.P. Cartmell, Regular and chaotic dynamics of a discontinuously nonlinear rotor system, *Chaos, Solitons and Fractals* 13 (6) (2002) 1231–1242.
[35] A. Paiva, M.A. Savi, An overview of constitutive models for shape memory alloys, *Mathematical Problems in Engineering* (2006) 1–30. Article ID56876.
[36] D.C. Lagoudas, Shape Memory Alloys: Modeling and Engineering Applications, Springer.
[37] M.A. Savi, A. Paiva, A.P. Baêta-Neves, P.M.C.L. Pacheco, Phenomenological modeling and numerical simulation of shape memory alloys: a thermo-plastic-phase transformation coupled model, *Journal of Intelligent Material Systems and Structures* 13 (5) (2002) 261–273.
[38] R.A.A. Aguiar, M.A. Savi, P.M.C.L. Pacheco, Experimental and numerical investigations of shape memory alloy helical springs, *Smart Materials and Structures* 19 (2) (2010) 1–9. Article 025008.